Propagation of Z-mode and whistler-mode emissions observed by Interball 2 in the nightside auroral region

O Santolik, François Lefeuvre, Michel Parrot, Jean-Louis Rauch

JOURNAL OF GEOPHYSICAL RESEARCH, VOL. 106, NO. A10, PAGES 21,137-21,146, OCTOBER 1, 2001

Propagation of Z-mode and whistler-mode emissions observed by Interball 2 in the nightside auroral region

O. Santolík,[1,2] F. Lefeuvre, M. Parrot, and J. L. Rauch

Laboratoire de Physique et Chimie de l'Environnement, Centre National de la Recherche Scientifique Orléans, France

Abstract. A case study of VLF (very low frequency) natural emissions propagating at high altitude above the nightside auroral zone is presented. The analysis is based on data of the MEMO experiment on board the Interball 2 spacecraft. In its VLF band the device records waveforms of three magnetic and two electric field components covering a frequency range 1-20 kHz. Several analysis methods are applied in order to obtain the details on the wave propagation and mode structure and to identify possible source regions. We demonstrate that observed band-limited emission consists of Z-mode and whistler-mode waves. Downgoing Z-mode waves are found just above the lower cutoff at the L=0 frequency. A possible source may be connected with the electron cyclotron resonance mechanism taking place in the nightside sector at altitudes above 21,000 km. Upgoing whistler-mode waves with upper cutoff at the local plasma frequency are probably generated by upgoing electrons in the auroral region at altitudes lower than the actual satellite position, i.e., below 18,000 km.

1. Introduction

Three main types of natural wave emissions were so far observed from spacecraft in the high-altitude auroral zone: auroral hiss, Z-mode radiation, and auroral kilometric radiation (AKR) [*Gurnett et al.*, 1983]. Ground-based observations also show other phenomena occurring at higher frequencies, such as MF bursts [*Weatherwax et al.*, 1994] and auroral roar emissions [*Yoon et al.*, 2000]. In the present paper we will analyze spacecraft data in the VLF range, and thus we will be concerned with the whistler-mode auroral hiss and with the Z-mode radiation. Two basic generation mechanisms have been proposed for auroral Z-mode radiation: the Landau resonance with downgoing auroral electrons [*Gurnett et al.*, 1983] and the loss cone driven cyclotron maser mechanism similar to that for AKR [*Hewitt et al.*, 1983; *Omidi et al.*, 1984]. Auroral hiss observed at high altitudes is generally considered to be generated by the Landau resonance with auroral electron beams [*Gurnett et al.*, 1983]. In the past, the emissions of auroral hiss and Z-mode radiation were mainly examined from the time-frequency power spectrograms. Waveform data recorded on board Interball 2 allow more detailed analyses. The MEMO (Mesures Multicomposantes des Ondes) experiment [*Lefeuvre et al.*, 1998] measures the waveforms of several components of the electromagnetic field. In its ELF and VLF bands (0.05-1 and 1-20 kHz, respectively) it simultaneously records the data from three magnetic antennas and two electric antennas. In its HF band (30-200 kHz) it measures waveforms of three magnetic antennas and one electric antenna.

In the VLF range we thus dispose of the full vector of the magnetic field and of simultaneously measured data of two electric components. Although several methods exist to get propagation characteristics from both the magnetic and electric field data [e.g., *Lefeuvre et al.*, 1986], they cannot be used in this context, because they suppose a special orientation of the electric antennas with respect to the ambient magnetic field. We have thus recently revised these techniques, and we have newly developed several methods of wave propagation analysis of multicomponent data [*Santolík et al.*, 2001]. The aim of these techniques is to obtain (1) wave vector direction, (2) wave number or index of refraction, and (3) Poynting vector. We suppose that coupling of electric antennas to the plasma can be described by a single complex transfer function. This transfer function can also be estimated from the wave data.

As these techniques will be used in the present paper, their brief description is necessary to interpret the results. It will be given in section 2. As a complementary approach, we will use the wave distribution function (WDF) analysis [*Storey and Lefeuvre*, 1979], which will allow us to distinguish different wave modes. Section 3 will present the results of the analysis for a selected case of VLF emissions in the nightside auroral region. Theoretical analysis of wave

[1]Also at Faculty of Mathematics and Physics, Charles University, Prague, Czech Republic.

[2]Now at Department of Physics and Astronomy, University of Iowa, Iowa City, Iowa, USA.

Paper number 2001JA000038.
0148-0227/01/2001JA000038$09.00

propagation parameters for this case and processing of simulated data will be described in section 4. Section 5 will then show the results of the WDF analysis. Finally, section 6 will contain a discussion and brief conclusions.

2. Analysis Methods

2.1. Plane-Wave Analysis Using the Magnetic Field Vector Data

2.1.1. Incomplete wave vector direction. The plane of polarization of the magnetic field is always perpendicular to the wave vector direction. For a given magnetic field data we have two mutually antiparallel directions which agree with this condition. We can thus only estimate an incomplete wave vector direction with the sign ambiguity. We will use the method of *Means* [1972]. As the propagation properties of the plasma medium are symmetric with respect to the ambient magnetic field ($\boldsymbol{B}_0$), the results are best represented in a spherical system by two angles, θ (deviation from $\boldsymbol{B}_0$) and ϕ (azimuth around $\boldsymbol{B}_0$ having the zero value in the direction of increasing magnetic latitude). The method gives an ambiguous result with $\theta \leq 90°$, which may also indicate propagation in the antiparallel direction with $\theta' = 180° - \theta$ and $\phi' = 180° + \phi$.

2.1.2. Sense of polarization. We will also estimate a normalized parameter C_B defining the sense of circular or elliptical polarization [*Santolík et al.*, 2001]. The polarization is examined in the plane perpendicular to $\boldsymbol{B}_0$. Positive values of C_B correspond to the right-hand polarization (i.e., in the sense of the electron cyclotron motion), and negative values mean left-hand-polarized waves. The absolute value gives the statistical level of confidence, values above 3 or below -3 generally indicating a high confidence level.

2.1.3. Degree of polarization. The presence of a single plane wave will be tested by an estimator P of the degree of polarization obtained by the eigenanalysis of the magnetic spectral matrix, as defined by *Lefeuvre et al.* [1992]. A value above $\approx$0.8 means that there is no substantial discrepancy between the measured wave magnetic field and the hypothesis of a single plane wave.

2.2. Plane-Wave Analysis Using the Magnetic Field Vector Data and Two Electric Signals

2.2.1. Index of refraction. Having the magnetic field vector data and two electric signals, we can use Faraday's law in the frequency domain,

$$n\,(\boldsymbol{\kappa} \times \boldsymbol{E}) = c\boldsymbol{B}, \tag{1}$$

where $\boldsymbol{E}$ and $\boldsymbol{B}$ are the complex amplitudes of the wave electric and magnetic field, respectively, n is the index of refraction $n = k\,c/\omega$, k is the wave number, c is the speed of light, ω is the angular frequency, and $\boldsymbol{\kappa}$ is a unit vector defining the wave vector direction $\boldsymbol{\kappa} = \boldsymbol{k}/k$. Equation 1 can be used to simultaneously estimate the wave number and the hemisphere of propagation. The procedure is based on the transformation of the three-component magnetic field data to a Cartesian frame connected with the electric antennas [*Santolík et al.*, 2001].

The first result is the ratio $n/|Z|$, where $|Z|$ is the absolute value of the complex transfer function describing the coupling of electric antennas to the plasma. Supposing a known transfer function (or assuming it is unity), we can get the index of refraction n and subsequently the wave number k. On the other hand, with a known theoretical value of the refractive index, the transfer function can be estimated. However, without actually measuring Z by additional electronics connected to the electric antennas, it is often difficult to separate the transfer function from n. In the present paper we will always show the results for the ratio $n/|Z|$, and we will compare its values to the theoretical refractive index.

The method also gives us a phase shift Φ_b. For a given $\boldsymbol{\kappa}$, Φ_b directly reflects the phase shift due to the complex transfer function, $Z = |Z| \exp(i\Phi_b)$. When, as it is the case in the present paper, $\boldsymbol{\kappa}$ is originally estimated from the magnetic field data without knowing its correct sign (see section 2.1.1), Φ_b can be used to resolve that ambiguity. Supposing that the phase shift induced by Z is smaller than 90°, Φ_b defines the actual hemisphere of $\boldsymbol{\kappa}$. Φ_b values between -90° and +90° correspond to $\theta \leq 90°$, and Φ_b values below -90° or above +90° correspond to $\theta > 90°$.

2.2.2. Poynting vector. Faraday's law in the frequency domain can also be used to reconstruct the electric field vector from the magnetic field vector data and two electric components. Since both real and imaginary parts of $\boldsymbol{E}$ and $\boldsymbol{B}$ are mutually perpendicular vectors in (1), we can directly use this property to calculate the missing third electric field component [*Santolík et al.*, 2001]. In the present paper we use such completed information about the wave electric and magnetic fields to obtain the Poynting vector. We characterize it by the two following parameters: (1) angle deviation θ_P of the Poynting vector from $\boldsymbol{B}_0$ and (2) parameter D_b defined as the component of the Poynting vector which is parallel to $\boldsymbol{B}_0$, normalized by the statistical standard deviation of its estimate. We use here all three reconstructed electric field components unlike two similar methods also described by *Santolík et al.* [2001], and hence no principal restrictions of validity apply to obtained D_b values. $D_b > 0$ corresponds to $\theta_P \leq 90°$, and $D_b < 0$ corresponds to $\theta_P > 90°$. The absolute value of D_b indicates the relative level of confidence, values above 3 or below -3 indicating a high statistical confidence.

2.3. Wave Distribution Function Analysis

All the above methods provide us with parameters describing a plane wave, like wave vector, Poynting vector, or refractive index. They thus inherently suppose a very simple propagation model consisting of a single plane wave in a single wave mode. We will show that even if this is not exactly the case, the methods give reasonable average results. However, sometimes a more complex description of observed wave fields is necessary. This is the case when the waves simultaneously propagate with two or more wave vector directions, or if several wave modes are simultaneously present. The WDF then may serve to describe the wave propagation [*Storey and Lefeuvre*, 1979]. The WDF analysis allows us to consider an arbitrary distribution of

wave energy density over the different wave vector directions and wave modes. Here we estimate the WDF by the optimization method described as "model of discrete regions" by *Santolík and Parrot* [2000]. In order to maintain a reasonable number of optimized parameters, we estimate the WDF for $\theta \leq 90°$ in two cold-plasma wave modes, and we use the magnetic field data only. This implies that we cannot distinguish between any two antiparallel wave vector directions, as can be done with the plane-wave methods described in section 2.2. The two approaches (plane-wave and WDF analysis) are thus complementary in the present paper.

3. Analysis of Z-Mode and Whistler-Mode VLF Emissions

On November 9, 1996, between 2300 and 2340 UT the MEMO device recorded intense natural emissions in the VLF band. The multicomponent waveform data were recorded in short snapshots of 0.09 s, separated by ≈65-s data gaps. To select the snapshot for a detailed analysis we have used continuously recorded data of the NVK-ONCH device [*Mogilevski et al.*, 1998] on board Interball 2. The spectrogram shown in Plate 1 was created using a waveform measurement of an electric component between 2314 and 2326 UT when the satellite was located above the northern nightside auroral region. During this interval we can see band-limited emissions with both lower and upper characteristic cutoffs. The ≈1-min periodic variations of the upper and lower cutoffs and of the wave intensity are connected to the spacecraft spin.

Figure 1 presents some results of a detailed multicomponent analysis of one MEMO snapshot, recorded when the maximum wave intensity was observed. The data were measured from 2320:10 UT, and at this moment the satellite was at an invariant latitude of 73.8°, on 0310 MLT, and at an altitude of 18,038 km.

Both distinct cutoffs are seen in the electric spectrum in Figure 1b. They can also be distinguished in the magnetic spectrum in Figure 1a. Note, however, that near the upper cutoff the level of the magnetic field fluctuations decreases very close to the level of the background noise. Examination of the magnetic field polarization reveals prevailing left-hand elliptic polarization in the frequency band 3.5 – 5 kHz and prevailing right-hand elliptic polarization in the frequency band 6 – 10 kHz (Figure 1c). This may be explained by the presence of left-hand-polarized Z-mode waves in the lower-frequency band and right-hand whistler-mode waves in the higher-frequency band. Supposing that the plasma density decreases with altitude and that the plasma frequency is lower than the gyrofrequency, the observed cutoffs may also be explained by the presence of these wave modes [*Lefeuvre et al.*, 1998]. We obtain the lower cutoff if the left-hand-polarized Z-mode waves are downgoing, and, similarly, the upper cutoff can be explained by the principal resonance of whistler mode if the waves in the higher-frequency band are upgoing (see also section 4).

Propagation analysis is needed to verify this hypothesis. Figure 1e shows that waves propagate at large angles with respect to $\boldsymbol{B}_0$. In the frequency band 3.5 – 5 kHz the estimates by the method of *Means* [1972] give wave vectors with θ growing from ≈45° up to ≈80°. In the same band the Poynting vector is also found with a growing inclination from $\boldsymbol{B}_0$ but always at angles lower by 10° – 20° comparing to the wave vector direction. The estimate of D_b and the estimate of Φ_b clearly indicate downgoing propagation in this frequency interval, and the value of $n/|Z|$ grows from ≈0.1 to 0.2.

In the band 6 – 10 kHz the method of *Means* [1972] again gives θ between 50° and 80°, but a decreasing trend can be noted below 9.5 kHz. The Poynting vector is here found growing from ≈60° (downgoing propagation) up to 90°–100° (upgoing propagation) near 10 kHz. This is consistent with estimates of D_b, which indicate upgoing waves near 10 kHz, but at a lower level of confidence. Values of Φ_b clearly show upcoming propagation for 6 – 8 kHz, downgoing waves between 7 and 9 kHz, and again upcoming propagation above 9 kHz. The values of $n/|Z|$ fluctuate around 0.1 at frequencies between 6 and 10 kHz.

The results of the propagation analysis thus agree with the hypothesis, explaining the observed cutoffs and polarization reversal by the presence of downgoing Z-mode waves in the lower-frequency band and upcoming whistler-mode waves in the higher-frequency band.

4. Comparison With Theoretical Properties of Wave Propagation

To further check this hypothesis, we have calculated theoretical properties of both Z mode and whistler mode using the cold-plasma approximation. We have used an experimentally determined electron gyrofrequency f_g=27 kHz. The plasma frequency f_p=10.5 kHz was estimated from the observed upper cutoff supposing that this cutoff is due to the principal resonance of upcoming whistler-mode waves [*Persoon et al.*, 1988]. With these plasma parameters we obtain a theoretical prediction for the lower cutoff of the downgoing Z-mode waves at a frequency of 3.6 kHz. At this frequency the L parameter of *Stix* [1992] becomes zero, and the left-hand-polarized Z mode is cut off. This is shown in Plate 2a while the above discussed theoretical polarization properties of the Z-mode and whistler-mode waves are shown in Plates 2b and 2e. The theoretical value of the Z-mode lower cutoff is thus found near the lower cutoff really observed in the frequency spectra. This provides further support for our interpretation.

The behavior of the propagation parameters obtained from multicomponent data in the frequency band 3.6 – 5 kHz also agrees with the theoretical properties of the Z mode. The angular difference of 10° – 20° between the wave vector and the Poynting vector (Figure 1e) is well predicted by the theory (Plate 2c and Figures 2 and 3). The theoretically predicted refractive index is below 0.73 in this frequency band, which is also roughly comparable to the observed values of $n/|Z|$.

The experimental results show that throughout the fre-

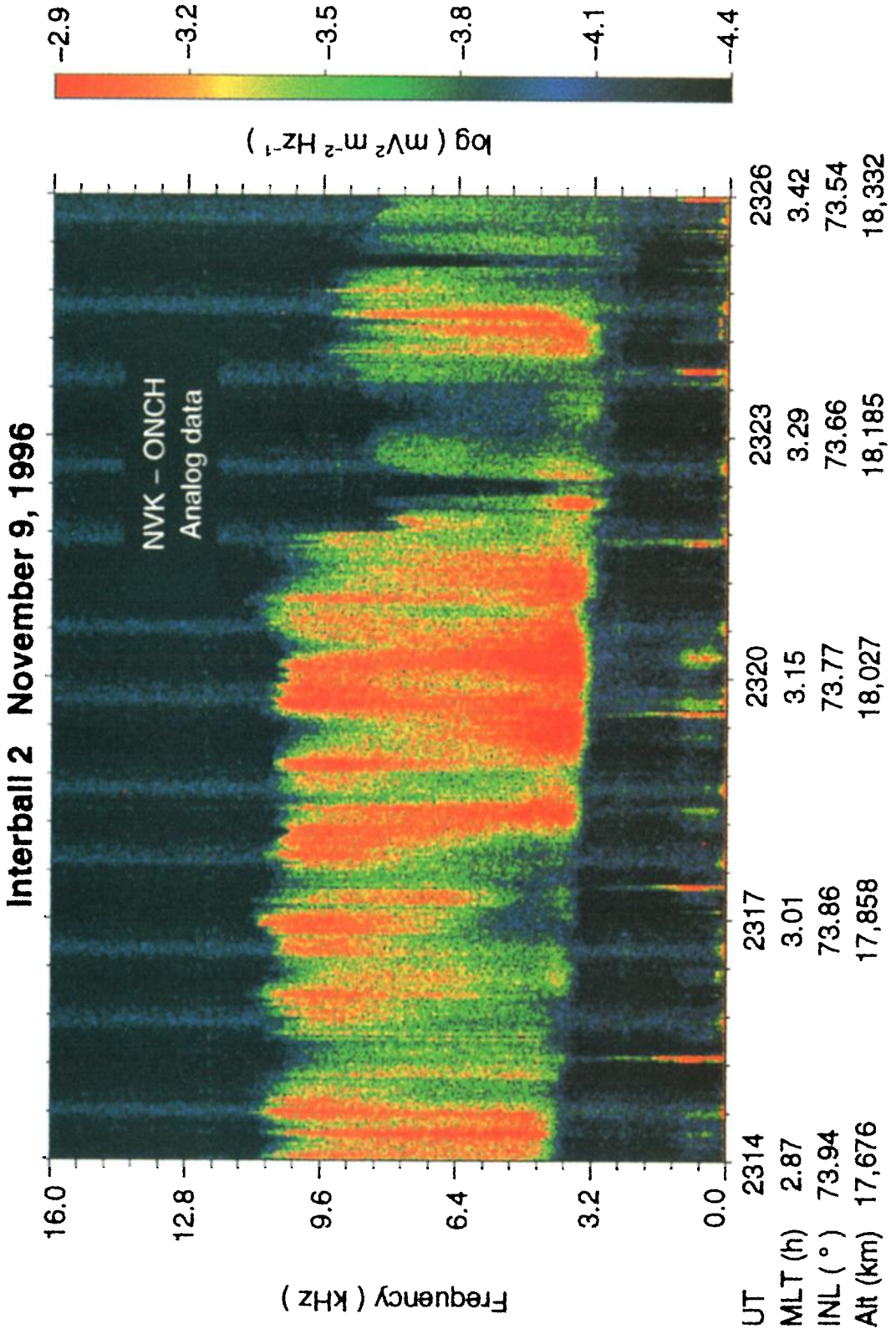

Plate 1. Power spectrogram of the electric field recorded in the VLF band on November 9, 1996. Magnetic local time (MLT), invariant latitude (INL), and altitude (Alt) are on the bottom.

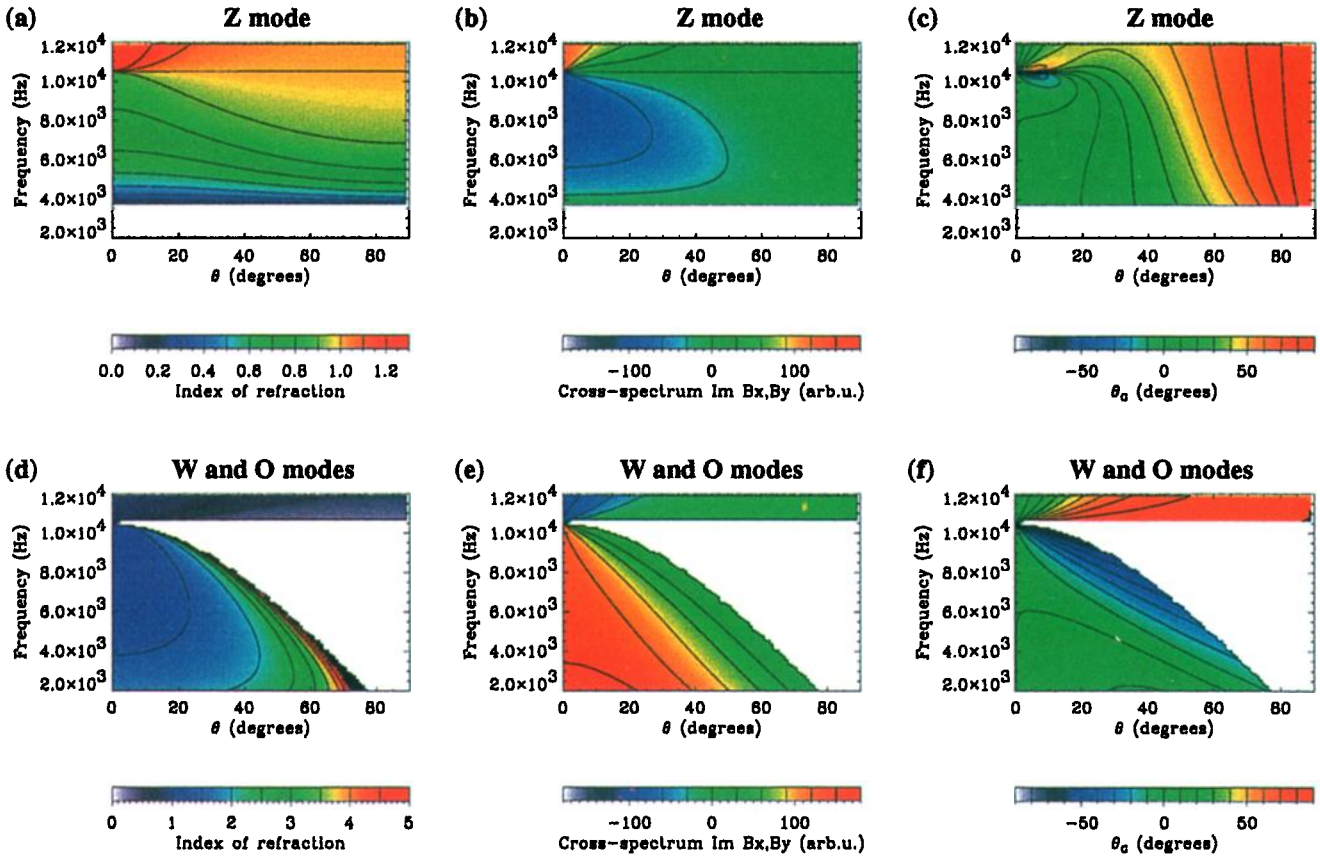

Plate 2. (a-f) Theoretical characteristics of wave propagation supposing $f_{pe} = 10.5$ kHz. Three selected parameters are color-coded as a function of θ and frequency. Z mode is on the top (Plates 2a, 2b, and 2c); whistler and ordinary modes are on the bottom (Plates 2d, 2e, and 2f). Plates 2a and 2d show the refractive index. Plates 2b and 2e represent the imaginary part of the cross spectrum between two magnetic components in the plane perpendicular to $\boldsymbol{B}_0$. Negative values correspond to the left-hand polarization; right-hand polarization is expressed by positive values. Plates 2c and 2f show the inclination of the Poynting vector from $\boldsymbol{B}_0$.

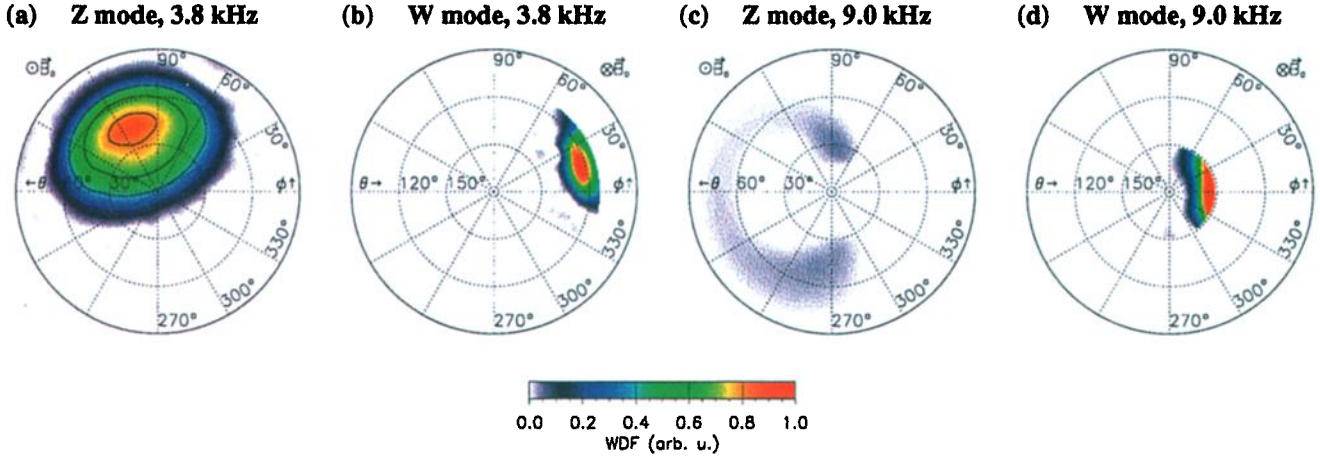

Plate 3. Results of simultaneous optimization of the WDF for both Z-mode (Plates 3a and 3c) and whistler mode (Plates 3b and 3d). The frequencies are 3.8 kHz (Plates 3a-3b) and 9.0 kHz (Plates 3c-3d). In all panels the WDF is plotted using the same color scale, shown on the bottom.

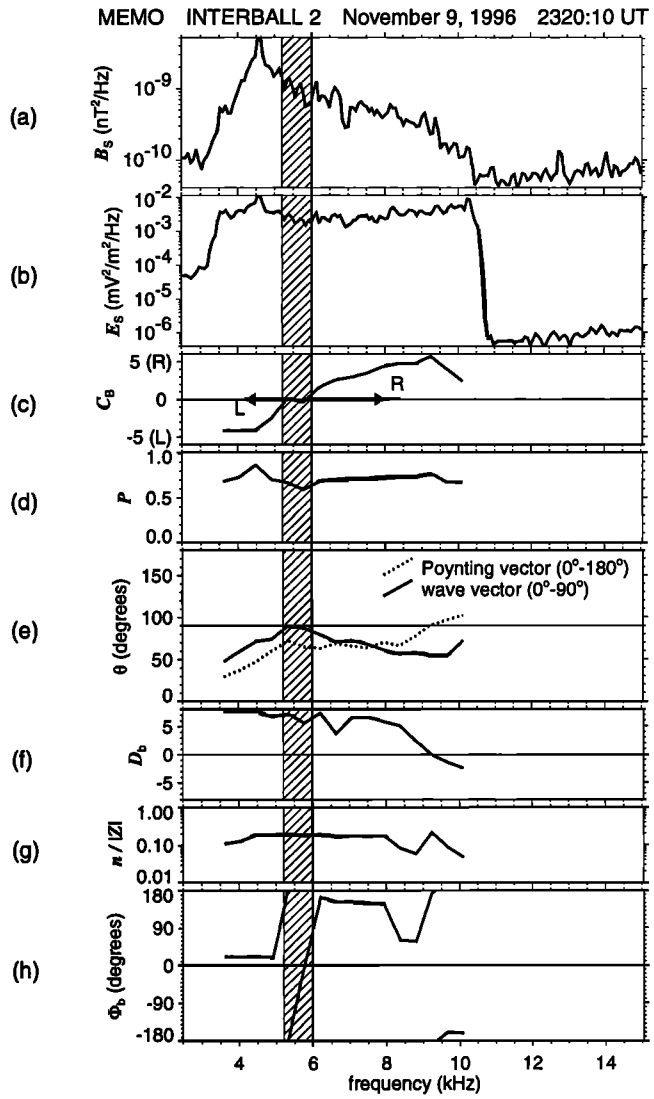

Figure 1. (a-h) Analysis of Z-mode and whistler-mode VLF emissions in the frequency interval 2.5 – 15 kHz. (a) Sum of the three magnetic autopower spectra. (b) Sum of the two electric autopower spectra. (c) Sense of polarization. (d) Degree of polarization. (e) Deviation θ of the wave vector direction from the ambient magnetic field $\boldsymbol{B}_0$ by the method of *Means* [1972] (solid line) and the same angle for the Poynting vector (dotted line). (f) Estimate D_b of the parallel component of the Poynting vector normalized by its standard deviation. (g) Ratio of the wave refractive index and the transfer function. (h) Phase shift Φ_b from the Faraday's law. The area filled with oblique parallel lines shows the frequency interval where the polarization changes from the left-hand (L) to the right-hand (R) sense.

quency interval 3.6 – 10 kHz, we observe a polarization degree which often is below 0.8 (Figure 1d). This suggests that the original assumption on the presence of a single plane wave can be violated. In order to verify the results when the plane wave assumption is not valid, we have simulated Z-mode waves at 4.5 kHz using the WDF techniques.

First, we have supposed that the waves propagate in a divergent beam of wave vectors, described as a Gaussian peak on the WDF (Model of Gaussian peaks of *Santolík and Parrot* [2000]). The beam is centered at a direction defined by θ_0=50° and ϕ_0=110° and has an angular width Δ. For Δ approaching zero the beam reduces to a single plane wave at a given θ_0 and ϕ_0. For large Δ the waves propagate simultaneously at all downgoing directions, but no wave energy penetrates to the hemisphere of upgoing waves. The data have been simulated for the same configuration of antennas as in the real case presented in Figure 1. The results for Δ between 0° and 90° are shown in Figure 2. We can see that nearly all the parameters are not influenced by the violation of the plane wave hypothesis and that they always indicate the right hemisphere. Note, however, that the angle θ estimated by the method of *Means* [1972] rapidly decreases with the growing width of the peak. Note also that the degree of polarization decreases for a wide peak, as can be expected when the plane wave hypothesis is violated [*Pinçon et al.*, 1992].

Another situation which may invalidate the results is the simultaneous propagation of upcoming and downgoing waves. We expect that the methods should identify the hemisphere of propagation where we place more wave energy. This is verified in Figure 3. The analysis is done for two simulated plane waves, simultaneously propagating in mutually antiparallel directions at θ_1=50°, ϕ_1=110°, and θ_2=130°, ϕ_2=290°, respectively. The percentage (p) of energy density placed into each of the two waves is gradually changed from purely downgoing wave (p=0%) to purely upcoming wave (p=100%). The simulated configuration of antennas is again the same as in the real case from Figure 1. The main result is that the propagation characteristics behave as expected. The estimated direction of the Poynting vector in Figure 3a reverses to the antiparallel direction just at the moment when p passes through 50%. This, obviously, is not the case of the results of the method of *Means* [1972], which always gives $\theta \leq 90°$. The estimate of D_b (Figure 3b) changes the sign when p is 50%. The phase Φ_b (Figure 3d) also always indicates the right hemisphere of prevailing propagation. The wave refractive index (Figure 3c) is substantially overestimated when the plane wave hypothesis is clearly invalid, i.e., when the wave energy placed to both hemispheres becomes comparable. Note that the exactly antiparallel plane waves were chosen for the sake of simplicity. This choice allowed us to avoid effects on the wave magnetic field: Both amplitudes and relative phases of the magnetic components are the same for the two antiparallel plane waves and remain unchanged when the two waves propagate simultaneously. As a consequence, the degree of polarization, calculated without taking into account the wave electric field, is always unity even when the waves simultaneously propagate in the two oposite directions. If we consider the case when the two plane waves are not antiparallel, the degree of polarization will be less than unity, as in the simulation shown in Figure 2. Also, effects connected to a different group velocity of the two waves can take place, resulting in a switch between detected directions at a different ratio of energy density placed into each of the two waves.

In the higher-frequency band (6 – 10 kHz) of the VLF

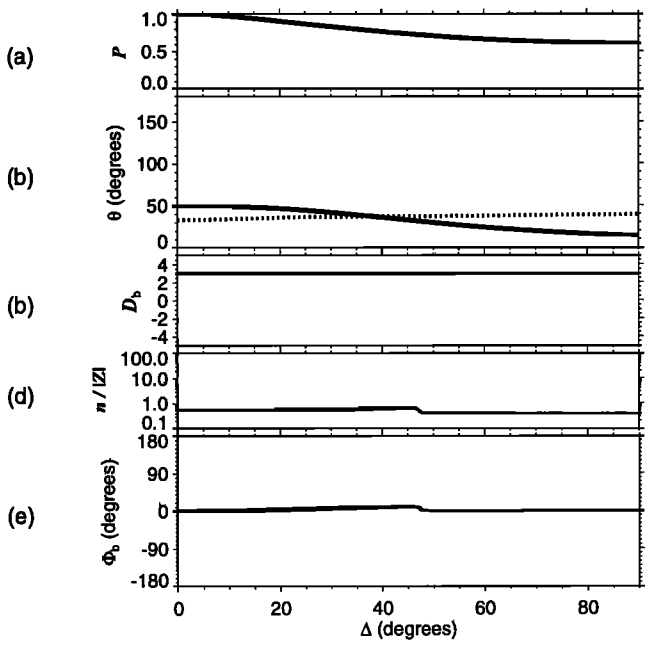

Figure 2. (a-e) Analysis of the influence of the plane wave hypothesis for Z mode at 4.5 kHz. The simulated results are a function of the width Δ of a Gaussian peak on the wave distribution function for the VLF case on November 9, 1996. The parameters shown are the same as those in Figures 1d-1h.

case of November 9, 1996, right-hand elliptic polarization of the wave magnetic field suggests the presence of whistler-mode waves. Theoretical parameters of this mode are shown in Plates 2d-2f. In the frequency band below f_p =10.5 kHz, whistler-mode waves propagate inside a resonance cone which rapidly closes when we approach the principal resonance at f_p. For example, at a frequency of 6 kHz the resonance angle (θ_R) is 53°, at 9 kHz it decreases to 29°, and it goes to zero at f_p. Naturally, the wave vector cannot be inclined from $\boldsymbol{B_0}$ by angles larger than θ_R. This is, however, the case of results of the method of *Means* [1972] presented in Figure 1e (recall that the observed θ values are between 50° and 80° in this frequency band). The Poynting vector may be theoretically found at large angles for the whistler-mode waves in this frequency range (up to 60° at 9 kHz), but the observed values between 60° and 100° are again inconsistent with the theory.

We have verified that the observed discrepancies are not artificially introduced by our analysis procedures; these methods well reproduce the theoretical predictions when used with simulated data (not shown). Note in this context that simple methods to estimate the parallel component of the wave vector and Poynting vector from only one or two electric components [*Santolík et al.*, 2001] cannot be used in the present case. The waves have a large parallel component of the electric field, and the simulation shows that these methods may give misleading results, depending on mutual orientation of the wave vector with respect to the antennas. The method that uses the reconstructed electric field vector (Figure 1f), however, gives correct results. These verifications indicate that the observed differences must either be connected to wrong assumptions of the theoretical analysis or to violation of the underlying hypothesis of the plane-wave methods.

5. WDF Analysis

In section 4 we have shown that some violations of the plane-wave hypothesis do not substantially disturb the resulting wave vector. However, a possible multimodal structure of the emission cannot be described by these plane-wave methods. This may be a possible reason for the observed discrepancy between the observed wavevector directions and the theoretical properties of the whistler mode in the higher-frequency band. We have thus allowed the WDF optimization procedure to distribute the wave energy between the two possible modes in order to best satisfy the constraints imposed by the observed data. The results are shown in Plates 3a-3d for frequencies of 3.8 and 9 kHz, respectively, with the analysis bandwidth of 0.3 kHz in both cases.

Each of Plates 3a-3d represents a WDF in a polar diagram, where the distribution of the wave energy density is plotted with respect to the polar angle θ and the angle azimuth ϕ. Recall that the WDFs are obtained from the magnetic field only, and hence we cannot separate WDF values from the two mutually antiparallel directions. Following the indications, obtained by the plane-wave methods that involve both magnetic and electric field, we choose to represent the Z-mode waves in the hemisphere where $\theta \leq 90°$ and the whistler-mode waves in the hemisphere of $\theta > 90°$.

An important result of this analysis is the ratio of integral wave energy density, which is 90% of Z mode and 10% of

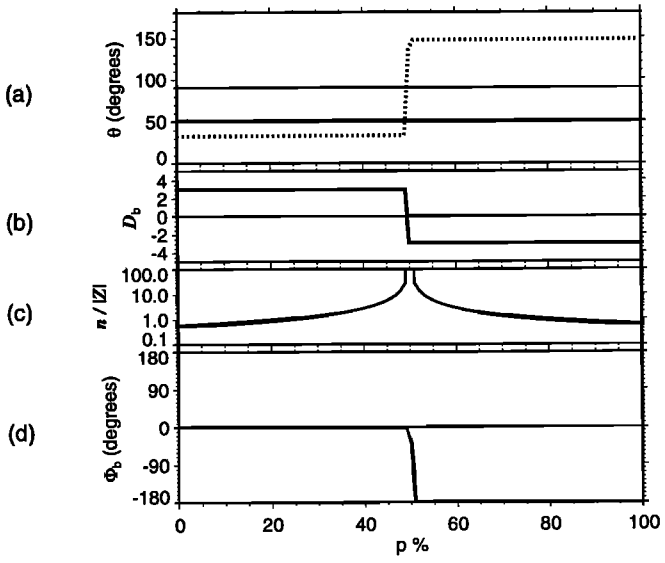

Figure 3. (a-d) Analysis of simulated Z-mode waves simultaneously propagating in two antiparallel directions at 4.5 kHz. Results are plotted as a function of the percentage p of the energy density of the upcoming wave. The parameters shown are the same as those in Figures 1e-1h.

whistler mode at 3.8 kHz, whereas in the higher-frequency band at 9 kHz we observe a majority of the whistler mode (81%) and a smaller fraction of the Z mode (19%). These wave energy ratios are not a priori imposed but come out of the WDF optimization procedure and thus are defined by the data. For the whistler-mode waves the peaks of wave energy density are always concentrated near the resonance cone. Their angle azimuth indicates propagation near the plane of the local magnetic meridian, with wave vectors pointing toward higher L shells provided that the waves are upcoming. Note that this WDF analysis is based on the cold-plasma theory, and no whistler-mode energy density can be obtained outside the resonance cone.

The peak of Z-mode radiation is found near $\theta = 40°$ at 3.8 kHz. This well agrees with the plane-wave results (Figure 1) at that frequency. As the waves are downgoing, the values of the angle azimuth ϕ where the peak is found correspond to waves propagating perpendicularly with respect to the local magnetic meridian, from the nightside sector (lower MLT). The peak WDF values are nearly the same for both modes at this frequency. However, the peak of the Z-mode waves is much larger in effective area, resulting in a much larger integral energy density. At 9 kHz the Z-mode waves are also spread over a large interval of wave vector directions. Although the WDF values are small, the integration gives a nonnegligible fraction of Z-mode waves. Besides a possible contamination by a background noise mentioned in section 3, the presence of Z-mode waves might be another possible reason of the discrepancy between θ values obtained by plane-wave methods at this frequency and the whistler-mode theory. As the residual Z-mode waves carry a large magnetic component, their presence at large θ may perturb the results of the method of *Means* [1972] and the determination of the Poynting vector.

6. Discussion and Summary

In the lower-frequency band between 3.6 and 5 kHz we clearly see the downgoing Z-mode waves (as supposed by *Lefeuvre et al.* [1998]), and theoretical predictions of different wave properties are consistent with the observations. This provides strong evidence that the Z-mode emissions come from higher altitudes. This scenario must be completed by the reflection of the Z-mode waves above the L=0 cutoff frequency. As the waves do not propagate parallel to $\boldsymbol{B}_0$, we may not necessarily observe a large fraction of the reflected waves at the actual satellite position. The angle azimuth ϕ obtained by the method of *Means* [1972] indicates that the reflected waves further propagate toward the morning sector.

Following *Gurnett et al.* [1983], the generation mechanism may be connected with a direct resonant interaction with downgoing electron beams. Since the Z-mode resonance cone appears only at frequencies between the local electron gyrofrequency (f_{ge}) and the upper hybrid frequency, an estimate of the altitude of such a source region is ≈36,000 km, supposing it is at the same invariant latitude as the observation point and assuming that the upper hybrid frequency is close to f_{ge}. Similar altitudes are required if the electron cyclotron resonance mechanism [*Tsurutani and Lakhina*, 1997] is considered. The calculations of *Hewitt et al.* [1983] show the possibility of Z-mode generation above f_{ge} by upgoing loss cone electrons. The unstable wave vectors are directed nearly perpendicular to $\boldsymbol{B}_0$ and upward, but, owing to properties of the Z mode at these frequencies, the corresponding group velocities are found to be directed obliquely downward. The group velocity, however, tends to be perpendicular to $\boldsymbol{B}_0$ when the wave propagates down to the altitude where its frequency approaches to f_{ge}. This mechanism thus encounters difficulties to explain propagation to lower altitudes. Taking into account realistic particle distributions and relativistic effects, the study of *Omidi et al.* [1984] shows that the generation can also take place slightly below f_{ge}. However, the downward propagation near the L=0 cutoff may again be hardly explained by this latter mechanism, because the unstable wave vectors correspond to a horizontal propagation perpendicular to $\boldsymbol{B}_0$, as found by the ray-tracing study by *Menietti and Lin* [1986].

On the other hand, ray tracing for the same mode but at higher frequencies done by *Horne* [1995] shows that a Z-mode wave may propagate downward quite near to the reflection point above the L=0 cutoff. This study is based on the generation mechanism of *Wu et al.* [1989], which predicts the maximum growth rate at frequencies around 0.8 f_g with downward directed wave vectors. This would in our case lead to a distant source region at an altitude of ≈33,000 km if the invariant latitude is similar as for the observation point (74°). If the source is at lower latitudes, its altitude would be lower, and it would go down to ≈21,000 km if the source is at the equator. This extreme possibility is, however, not very likely, because in that case we should observe poleward propagation. As our results rather indicate that the waves propagate toward higher MLT, without any prevailing poleward component, we suppose that the source region is on the nightside at higher latitudes. A ray-tracing study would be necessary to obtain more quantitative results. A weak point of this hypothesis is that the theory of *Wu et al.* [1989] was designed to explain ground-based observations of waves at frequencies above 150 kHz [*Benson et al.*, 1988], which are supposed to be generated in the auroral region at altitudes below 6500 km [*Ziebell et al.*, 1991]. Further analysis is needed to examine the critical parameters of this theory (ratio of the electron gyrofrequency to the plasma frequency, relative abundance of energetic electrons, their characteristic energy, and the shape of their distribution function) at altitudes above 18,000 km. As the local plasma frequency is above the frequency of observed Z-mode waves, we must also take into account the possibility of generation by an unknown mechanism near the local plasma frequency suggested by *Hashimoto and Calvert* [1990]. In that case the source region would also be above the observation point, supposing that the plasma density decreases with the altitude. *Hashimoto and Calvert* [1990] and *Calvert and Hashimoto* [1990], however, supposed upward Z-mode propagation,

consistently with their ray-tracing study. This does not agree with our results.

The pronounced upper cutoff seen in the electric field spectra is well explained provided that upgoing whistler waves carry the majority of wave power at those frequencies. The cutoff is then local, and it is situated at the plasma frequency [*Persoon et al.*, 1988]. With this assumption we obtain a good agreement between theoretically predicted lower cutoff of downgoing Z-mode radiation and the observed spectrum. The power spectra thus allow a self-consistent interpretation. However, in the higher-frequency band between 6 and 10 kHz the interpretation in terms of the wave propagation is much less straightforward. The presence of a nonnegligible fraction of Z-mode waves may explain the discrepancy between θ values obtained by plane-wave analysis and the whistler-mode theory. Another possible reason could be that near the upper cutoff at 10.5 kHz the wave magnetic field (Figure 1a) becomes weak, and the background noise may disturb the analysis. This is consistent with theoretical results showing that approaching the principal resonance of the whistler mode at the local plasma frequency, the wave magnetic field of whistler-mode waves weakens. A possible explanation could also be connected to modifications of the dispersion relation induced by a hot-plasma component. These effects are expected to be stronger near (or outside) the cold-plasma resonance cone where the phase velocity decreases, but their detailed study is beyond the scope of this paper.

Another problem is that the whistler-mode wave should prevail in the whole higher-frequency band 6-10 kHz, and the Poynting vector is directed upward only in a much narrower frequency interval above 9 kHz and below the upper cutoff (Figure 1e). Interpretation of the Poynting vector, however, must account for the difference of the group velocity of the whistler- and Z-mode waves. As the whistler-mode waves are found near the resonance cone, their group velocity is significantly lower than that of the Z-mode waves. This is obtained from the results of the cold-plasma theory (not shown) similar to those presented in Plate 2. When the two modes propagate simultaneously, the Poynting flux of the Z-mode waves can be higher, even if the whistler-mode waves have a higher energy density. To back up these considerations quantitatively, we have calculated theoretical fields of simultaneously propagating upgoing whistler-mode wave and downgoing Z-mode wave at a frequency of 9 kHz. Propagation of the two modes was simplified to two antiparallel plane waves, both deviated by 25° from $\boldsymbol{B}_0$. The relative energy density contained in each mode was gradually changed, and the Poynting vector was calculated by the same method as that in Figure 1e. As expected, the total Poynting flux was downward even if the energy density of the upgoing whistler-mode wave was larger than that of the Z-mode wave. Upward flux was found only when the relative fraction of the Z mode decreased below 15%. This is close to the ratio of energy density of the two modes found at 9 kHz by the WDF analysis. Simultaneous presence of both modes found by that method thus again can help to explain the observations.

Our analysis provides us with strong indications that below the upper cutoff the wave field is in majority composed of upgoing whistler-mode waves propagating in the vicinity of the resonance cone near the plane of the local magnetic meridian. The source of upgoing whistler waves is probably located in the auroral region at lower altitudes. The waves can be then generated by Landau resonance with the upgoing low-energy electron beams near the whistler-mode resonance cone at altitudes above ≈4500 km [*Gurnett et al.*, 1983]. We cannot, however, completely exclude the possibility that a part of the observed whistler-mode waves arises from mode conversion at the local plasma frequency from the downward propagating Z-mode radiation. In that case the Z-mode radiation in the lower-frequency band would represent waves remaining in the original mode, probably because they could not reach the radio window [*Budden*, 1985] where the conversion to the whistler mode may take place. This mechanism cannot, however, be the only one acting, because it would have difficulties in explaining the observed upper cutoff.

On the basis of the above presented wave propagation analysis of a broadband VLF emission observed in the nightside auroral region, we can summarize our interpretation as follows:

1. A complex system of VLF emissions observed on November 9, 1996, consists of downgoing Z-mode waves above the local L=0 cutoff and upgoing whistler-mode emissions below the principal resonance at the local plasma frequency. The WDF analysis shows 90% of Z-mode waves above the lower cutoff and 81% of whistler-mode waves below the upper cutoff.

2. The Z-mode waves come from regions above the observation point (altitude of 18,000 km) and from the nightside sector (MLT lower than 0310). The waves can be generated by a resonant interaction (Landau or electron cyclotron) with energetic electrons at a source altitude above 21,000 – 33,000 km.

3. The whistler-mode waves propagate from altitudes below the satellite position, and they propagate near the plane of the local magnetic meridian. The waves probably originate from the auroral hiss emissions [*Gurnett et al.*, 1983] generated by Landau resonance with upgoing electron beams.

Acknowledgments. We thank C. Béghin and L. R. O. Storey for helpful discussions on the behavior of electric antennas, and J.-Y. Brochot, who helped us with the processing of the MEMO data. This work was supported by the French-Czech program Barrande 98039/98055 and by the international program of scientific cooperation (PICS) 469 with the joint Czech Grant Agency grant 205/01/1064. O. Santolík acknowledges the support of the Czech Grant Agency grant 205/00/1686.

Janet G. Luhmann thanks Gurbax S. Lakhina and another referee for their assistance in evaluating this paper.

References

Benson, R. F., M. D. Desch, R. D. Hunsucker, and G. J. Romick, Ground-level detection of low- and medium-frequency auroral radio emissions, *J. Geophys. Res.*, *93*, 277–283, 1988.

Budden, K. G., The Propagation of Radio Waves, Cambridge Univ.

Press, New York, 1985.
Calvert, W., and K. Hashimoto, The magnetoionic modes and propagation properties of auroral radio emissions, *J. Geophys. Res., 95*, 3943–3957, 1990.
Gurnett, D.A., S.D. Shawhan, and R.R. Shaw, Auroral hiss, Z mode radiation, and auroral kilometric radiation in the polar magnetosphere: DE 1 observations, *J. Geophys. Res., 88*, 329–340, 1983.
Hashimoto, K., and W. Calvert, Observation of the Z mode with DE1 and its analysis by three dimensional ray tracing, *J. Geophys. Res., 95*, 3933–3942, 1990.
Hewitt, R. G., D. B. Melrose, and G. A. Dulk, Cyclotron maser emission of auroral Z mode radiation, *J. Geophys. Res., 88*, 10,065–10,071, 1983.
Horne, R. B., Propagation to the ground at high latitudes of auroral radio noise below the electron gyrofrequency, *J. Geophys. Res., 100*, 14,637–14,645, 1995.
Lefeuvre, F., Y. Marouan, M. Parrot, and J.L. Rauch, Rapid determination of the sense of polarization and propagation for random electromagnetic wave fields: Application to GEOS1 and AUREOL3 data, *Ann. Geophys., 4*, 457–468, 1986. (Correction, *Ann. Geophys., 5*, 251, 1987.)
Lefeuvre, F., J.L. Rauch, D. Lagoutte, J.J. Berthelier, and J.C. Cerisier, Propagation characteristics of dayside low-altitude hiss: Case studies, *J. Geophys. Res., 97*, 10,601–10,620, 1992.
Lefeuvre, F., M. Parrot, J.L. Rauch, B. Poirier, A. Masson, and M. Mogilevsky, Preliminary results from the MEMO multicomponent measurements of waves on-board Interball 2, *Ann. Geophys., 16*, 1117–1136, 1998.
Means, J. D., Use of the three-dimensional covariance matrix in analyzing the polarization properties of plane waves, *J. Geophys. Res., 77*, 5551–5559, 1972.
Menietti, J. D., and C. S. Lin, Ray tracing survey of Z mode emissions from source regions in the high-altitude auroral zone, *J. Geophys. Res., 91*, 13,559–13,568, 1986.
Mogilevsky, M.M., A.M. Golyavin, T.V. Aleksandrova, T.V. Romantsova, A.A. Rusanov, F. Jiříček, P. Tříska, and B. Poirier, Measurements of low frequency electromagnetic field onboard the Auroral probe satellite in the Interball project: The NVK-ONCH experiment, *Cosmic Res., 36*, 587-592, 1998.
Omidi, N., C. S. Wu, and D. A. Gurnett, Generation of auroral kilometric and Z mode radiation by the cyclotron maser mechanism, *J. Geophys. Res., 89*, 883–895, 1984.
Persoon, A. M., D. A. Gurnett, W. K. Peterson, J. H. Waite Jr., J. L. Burch, and J. L. Green, Electron density depletions in the nightside auroral zone, *J. Geophys. Res., 93*, 1871–1895, 1988.
Pinçon, J. L., Y. Marouan, and F. Lefeuvre, Interpretation of measurements of the polarization percentage for plasma waves, *Ann. Geophys., 10*, 82–95, 1992.
Santolík, O., and M. Parrot, Application of wave distribution function methods to an ELF hiss event at high latitudes, *J. Geophys. Res., 105*, 18,885–18,894, 2000.
Santolík, O., F. Lefeuvre, M. Parrot, and J.L. Rauch, Complete wave-vector directions of electromagnetic emissions: Application to Interball-2 measurements in the nightside auroral zone, *J. Geophys. Res.*, in press, 2001.
Stix, T. H., *Waves in Plasmas*, Am. Inst. of Phys., New York, 1992.
Storey, L. R. O., and F. Lefeuvre, The analysis of 6-component measurement of a random electromagnetic wave field in a magnetoplasma, 1, The direct problem, *Geophys. J. R. Astron. Soc., 56*, 255–270, 1979.
Tsurutani, B. T., and G. S. Lakhina, Some basic concepts of wave-particle interactions in collisionless plasmas, *Rev. Geophys., 35*, 491–561, 1997.
Weatherwax, A. T., J. LaBelle, and M. L. Trimpi, A new type of auroral radio emission observed at medium frequencies (~1350-3700 kHz) using ground-based receivers, *Geophys. Res. Lett., 21*, 2753–2756, 1994.
Wu, C. S., P. H. Yoon, and H. P. Freund, A theory of electron cyclotron waves generated along auroral field lines observed by ground facilities, *Geophys. Res. Lett., 16*, 1461–1464, 1989.
Yoon, P. H., A. T. Weatherwax, and J. LaBelle, Discrete electrostatic eigenmodes associated with ionospheric density structure: Generation of auroral roar fine frequency structure, *J. Geophys. Res., 105*, 27,589–27,596, 2000.
Ziebell, L. F., C. S. Wu, and P. H. Yoon, Kilometric radio waves generated along auroral field lines observed by ground facilities: A theoretical model, *J. Geophys. Res., 96*, 1495–1501, 1991.

F. Lefeuvre, M. Parrot, and J. L. Rauch, Laboratoire de Physique et Chimie de l'Environnement, CNRS, 3A, Avenue de la Recherche Scientifique, F-45071 Orléans cedex 02, France. (lefeuvre@cnrs-orleans.fr; mparrot@cnrs-orleans.fr; jlrauch@cnrs-orleans.fr)

O. Santolík, Department of Physics and Astronomy, University of Iowa, Iowa City, IA 52242-1479, USA. (ondrej.santolik@mff.cuni.cz)

(Received February 6, 2001; revised April 25, 2001; accepted April 25, 2001.)